# A modulated gradient model for large-eddy simulation: application to a neutral atmospheric boundary layer

Hao Lu,[1,*] Fernando Porté-Agel[1,2,†]
[1]Saint Anthony Falls Laboratory, Civil Engineering, University of Minnesota - Twin Cities, 2 Third Ave SE, Minneapolis, MN 55414, USA
[2]School of Architecture, Civil and Environmental Engineering, École Polytechnique Fédérale de Lausanne, Lausanne, Switzerland

January 6, 2010

**Abstract**

The subgrid-scale (SGS) parameterization represents a critical component of a successful large-eddy simulation (LES). It is known that in LES of high-Reynolds-number atmospheric boundary layer turbulence, standard eddy-viscosity models poorly predict mean shear in the near-wall region and yield erroneous velocity profiles. In this paper, a modulated gradient model is proposed. This approach is based on the Taylor expansion of the SGS stress, and uses local equilibrium hypothesis to evaluate the SGS kinetic energy. To ensure numerical stability, a clipping procedure is used to avoid local kinetic energy transfer from unresolved to resolved scales. Two approaches are considered to specify the model coefficient: a constant value of 1, and a simple correction to account for the effects of the clipping procedure on the SGS energy production rate. The model is assessed through a systematic comparison with well-established empirical formulations and theoretical predictions of a variety of flow statistics in a neutral atmospheric boundary layer. Overall, the statistics of the simulated velocity field obtained with the new model show good agreement with reference results and a significant improvement compared to simulations with standard eddy-viscosity models. For instance, the new model is capable to reproduce the expected log-law mean velocity profile and power-law energy spectra. Simulations also yield streaky structures and

*E-mail: hao.lu@live.com
†E-mail: fporte@umn.edu

near-Gaussian probability density functions of velocity in the near-wall region. It is found that using a constant coefficient of 1 yields a slightly excessive SGS dissipation, which is corrected when the coefficient is modified using the above mentioned correction.

# 1 Introduction

Large-eddy simulation (LES) of anisotropic turbulent flows has been an active and challenging field since the 1960s. In LES, large scales are explicitly resolved, while effects of subgrid-scales (SGS) are parameterized. SGS modeling is necessarily based on simple assumptions and phenomenological theories. Even though most SGS models assume a universal behavior of small scales, this assumption often breaks down due to flow anisotropy affecting the unresolved scales, for instance near the surface in high-Reynolds-number boundary layer flows. As a result, several studies [1, 2, 3, 4] have shown that simulation results are highly sensitive to the SGS model as well as to the grid resolution.

Most simulations of atmospheric boundary layer (ABL) turbulence have been achieved using eddy-viscosity based SGS models [5, 6, 7, 3]. The eddy-viscosity closure assumes a one-to-one correlation between the SGS stress tensor and the strain rate tensor, and locally employs the same eddy-viscosity for all directions. However, *a-priori* analysis of velocity fields obtained from experiments [8, 9] and direct numerical simulations (DNS) [10, 11] has confirmed the low correlation between the SGS stress tensor and the strain rate tensor. Studies of Khanna and Brasseur [12], Juneja and Brasseur [13], and Porté-Agel et al. [3] have also shown that on coarse grids eddy-viscosity models may induce large errors because they are not able to account for the strong flow anisotropy in the near-wall region. Moreover, eddy-viscosity models do not have the same rotation transformation properties as the actual SGS stress tensor, which is not material frame indifferent (MFI). Recent studies [14, 15, 11, 16] have revisited the importance of the MFI-consistency of the modeled SGS stresses. In LES of meso-scale and large-scale atmospheric turbulence including planetary rotation, eddy-viscosity models induce extra errors and yield unsatisfactory results, such as the incapability of capturing cyclone/anti-cyclone asymmetry in favor of cyclone [16]. In addition, eddy-viscosity models are by construction fully dissipative, and do not allow energy transfer from unresolved to resolved scales. However, such inverse energy transfer is known to occur, especially in anisotropic turbulence [17, 18].

Gradient models, also referred to as non-linear models, have been proposed since the late 1970s [19]. They are based on the Taylor expansion of the SGS stresses, $\tau_{ij} = \widetilde{u_i u_j} - \widetilde{u}_i \widetilde{u}_j = \widetilde{G}_{ij} + O(\Delta^4)$, where the gradient term is $\widetilde{G}_{ij} = \frac{\widetilde{\Delta}^2}{12}\left(\frac{\partial \widetilde{u}_i}{\partial x_k}\frac{\partial \widetilde{u}_j}{\partial x_k}\right)$ for isotropic Gaussian filter of size $\widetilde{\Delta}$. The model has several important advantages [8, 20, 21, 11]: (i) it does not require an extra filtering; (ii) it satisfies Galilean invariance and the modeled stress tensor is MFI-consistent with the actual SGS

stress tensor; (iii) at the *a-priori* test level, the analysis has shown the modeled SGS stresses exhibit good correlations with the actual SGS stresses over a wide range of filter sizes; (iv) it only relies on local velocity gradients and thus is easy to be applied to turbulent flows in complex geometries; and (v) it allows energy transfer from small to large scales. However, the standard gradient model has also one important limitation: when implemented in LESs, it hardly dissipates small-scale turbulence, as a result, simulations become numerically unstable.

Different schemes have been introduced to resolve this insufficient small-scale dissipation issue for high-correlation models. In 1980, Bardina et al. [22] introduced a mixed procedure, which is a linear combination of a scale-similarity model and an eddy-viscosity model. Vreman et al. [23] and Lu et al. [16] have also applied a similar mixed procedure with the gradient model and shown that mixed gradient models are able to capture disequilibrium and anisotropy effects. In 1994, Liu, Meneveau and Katz [8] revisited this energy cascade issue and recommended another meaningful choice, a clipping procedure, to control the amplitude of backward cascade induced by the model. Inconveniently, Vreman et al. [23] have reported that the modified (coupled with clipping) gradient model still does not provide sufficient SGS dissipation in simulations of mixing flows. We have also found a similar limitation of this scheme in simulations of ABL turbulence.

In an effort to improve the correlation as well as the magnitude of the SGS stress, Pomraning et al. [24] introduced a one-equation scheme, which models the SGS stresses as $\tau_{ij} = k_{sgs} C_{ij}$. The SGS kinetic energy, $k_{sgs} = \frac{1}{2}\left(\widetilde{u_i u_i} - \widetilde{u}_i \widetilde{u}_i\right)$, is calculated solving an additional prognostic equation. Note that the nondimensional tensor $C_{ij}$ must satisfy $C_{kk} = 2$. Applying the same model at the test filtering level and assuming scale invariance of $C_{ij}$, one can write $T_{ij} = \widetilde{\widetilde{u_i u_j}} - \widetilde{\overline{u}}_i \widetilde{\overline{u}}_j = K C_{ij}$. Integrating it into the Germano identity [25], one finds $L_{ij} = T_{ij} - \overline{\tau}_{ij} = K C_{ij} - \overline{k_{sgs} C_{ij}} \approx \left(K - \overline{k_{sgs}}\right) C_{ij}$, where $L_{ij} = \widetilde{\overline{u}_i \overline{u}_j} - \widetilde{\overline{u}}_i \widetilde{\overline{u}}_j$ is the Leonard stress. The resulting model has a simple algebraic expression, $\tau_{ij} = 2 k_{sgs} \left(\frac{L_{ij}}{L_{kk}}\right)$; the structure of $\tau_{ij}$ is extracted from the Leonard stress, and the magnitude of $\tau_{ij}$ is determined by the SGS kinetic energy. This model yields good agreement with filtered DNS data of low-Reynolds-number isotropic turbulence; however, it has some limitations, such as insufficient dissipation in high-Reynolds-number flow simulations, and the fact that the Leonard stress tensor is not MFI-consistent with the actual SGS stress tensor. To address those limitations, Lu et al. [11, 16] proposed and examined two revisions, that yielded outstanding results in LES of high-Reynolds-number isotropic and rotating turbulence. One revision is constructed using the gradient term $\widetilde{G}_{ij}$, therefore inheriting some of the features of gradient models. In *a-priori* tests [11], this model yields improved results (with respect to many other models) in terms of correlation and regression coefficients between measured and modeled components of the SGS stress tensor, components of the divergence of the SGS stress, and the SGS energy production term.

We focus on the development of a simple alternative to the standard eddy-

viscosity closure, and propose (in section 2) a computationally inexpensive modulated gradient model that uses the local equilibrium hypothesis to estimate the SGS kinetic energy and adopts a clipping procedure to avoid local energy transfer from unresolved to resolved scales. The performance of the modulated gradient model is tested in simulations of a high-Reynolds-number neutral ABL. Section 3 describes the governing equations and numerical setup, and section 4 presents the LES results. Section 5 summarizes the findings.

# 2 The modulated gradient model

Motivated by recent studies [11, 16], we propose a modulated gradient model as

$$\tau_{ij} = 2k_{sgs}\left(\frac{\widetilde{G}_{ij}}{\widetilde{G}_{kk}}\right) \ . \tag{1}$$

To account for the grid anisotropy (when $\widetilde{\Delta}_x$, $\widetilde{\Delta}_y$ and $\widetilde{\Delta}_z$ are not equal), $\widetilde{G}_{ij}$ is defined as

$$\widetilde{G}_{ij} = \frac{\widetilde{\Delta}_x^2}{12}\frac{\partial\widetilde{u}_i}{\partial x}\frac{\partial\widetilde{u}_j}{\partial x} + \frac{\widetilde{\Delta}_y^2}{12}\frac{\partial\widetilde{u}_i}{\partial y}\frac{\partial\widetilde{u}_j}{\partial y} + \frac{\widetilde{\Delta}_z^2}{12}\frac{\partial\widetilde{u}_i}{\partial z}\frac{\partial\widetilde{u}_j}{\partial z} \ . \tag{2}$$

The SGS kinetic energy $k_{sgs}$ is evaluated using the resolved velocities. To do that, we use the 'local' equilibrum hypothesis, which assumes a balance between SGS energy production $P$ and dissipation rate $\varepsilon$. SGS energy production is defined as $P = -\tau_{ij}\frac{\partial\widetilde{u}_i}{\partial x_j} = -\tau_{ij}\widetilde{S}_{ij}$. A simple evaluation of kinetic energy dissipation is $\varepsilon = C_\varepsilon\frac{k_{sgs}^{3/2}}{\widetilde{\Delta}}$, and the coefficient is assumed to be $C_\varepsilon = 1$ based on previous studies [26, 27]. Using the proposed model formulation (equation (1)) together with the local equilibrium hypothesis, one may obtain $k_{sgs} = \frac{4\widetilde{\Delta}^2}{C_\varepsilon^2}\left(-\frac{\widetilde{G}_{ij}}{\widetilde{G}_{kk}}\widetilde{S}_{ij}\right)^2$ and $\varepsilon = \frac{8\widetilde{\Delta}^2}{C_\varepsilon^2}\left(-\frac{\widetilde{G}_{ij}}{\widetilde{G}_{kk}}\widetilde{S}_{ij}\right)^3$. To ensure numerical stability, no local energy transfer from unresolved to resolved scales is allowed, which is consistent with the fact that dissipation rate is nonnegative, and thus

$$k_{sgs} = \begin{cases} \frac{4\widetilde{\Delta}^2}{C_\varepsilon^2}\left(-\frac{\widetilde{G}_{ij}}{\widetilde{G}_{kk}}\widetilde{S}_{ij}\right)^2 & \text{if } \widetilde{G}_{ij}\widetilde{S}_{ij} < 0 \\ 0 & \text{otherwise} \end{cases} \tag{3}$$

It is important to point out that the value of $C_\varepsilon = 1$ is based on the assumption of an averaged energy balance between SGS energy production and dissipation rate in the inertial subrange of high-Reynolds-number turbulence (see Ch. 13 of [28]). Considering that the clipping procedure eliminates the contribution of inverse energy transfer ($P < 0$), a value of $C_\varepsilon = 1$ is likely to overestimate the SGS energy transfer rate. Therefore, it is of interest to have a correction coefficient $C$ to modify $C_\varepsilon$ such that $\langle\varepsilon\rangle_{\mathbb{C}}$ can represent the actual dissipate rate more accurately, where the subscript '$\mathbb{C}$' denotes conditional average requiring $-\widetilde{G}_{ij}\widetilde{S}_{ij} \geq 0$. In the case of homogeneous boundary layers, like the one considered here, averaging is performed

over homogeneous directions (horizontal planes). A simple solution for $C$ is obtained, based on information contained in the resolved scales,

$$C = \sqrt{\left\langle \left( -\frac{\widetilde{G}_{ij}}{\widetilde{G}_{kk}} \widetilde{S}_{ij} \right)^3 \right\rangle_{\mathbb{C}} \cdot \left\langle \left( -\frac{\widetilde{G}_{ij}}{\widetilde{G}_{kk}} \widetilde{S}_{ij} \right)^3 \right\rangle^{-1}} \ . \tag{4}$$

Thus, an adjusted SGS kinetic energy to be used in the modulated gradient model is

$$k_{sgs} = \begin{cases} \frac{4\widetilde{\Delta}^2}{(C_\varepsilon\ C)^2} \left( -\frac{\widetilde{G}_{ij}}{\widetilde{G}_{kk}} \widetilde{S}_{ij} \right)^2 & \text{if } \widetilde{G}_{ij}\widetilde{S}_{ij} < 0 \\ 0 & \text{otherwise} \end{cases} \tag{5}$$

In summary, equations (1), (3), (4) and (5) form the basis of the new modulated gradient model. It should be noted that the model retains advantageous features of the standard gradient model and, in addition, it is expected to have improved dissipation characteristics. Next, the model is tested in simulations of the well-established case of a high-Reynolds-number turbulent boundary layer flow over a homogeneous surface. To isolate the effect of the correction given by equation (4) on the model performance, two versions of the model are tested: (i) a 'baseline' model that uses equation (3) (same as equation (5) with $C = 1$) to estimate the SGS kinetic energy; and (ii) a 'corrected' model that uses equation (4) to compute the correction coefficient $C$ and uses equation (5) to estimate the SGS kinetic energy.

# 3 Problem formulation

We use a modified LES code which has been used for other studies [29, 30, 3, 31, 32, 33]. The code solves the filtered Navier-Stokes equations

$$\frac{\partial \widetilde{u}_i}{\partial x_i} = 0 \ , \ \frac{\partial \widetilde{u}_i}{\partial t} + \frac{\partial \widetilde{u}_i \widetilde{u}_j}{\partial x_j} = -\frac{\partial \widetilde{p}}{\partial x_i} - \frac{\partial \tau_{ij}}{\partial x_j} + \widetilde{f}_i \ , \tag{6}$$

where $\widetilde{p}$ is the effective pressure, $\widetilde{f}_i$ is a forcing term, and the SGS stress tensor is $\tau_{ij} = \widetilde{u_i u_j} - \widetilde{u}_i \widetilde{u}_j$. The simulated flow is driven by a constant pressure gradient $-u_*^2/H$ in the x-direction. Since the Reynolds number is high, no near-ground viscous processes are resolved, and the viscous term is neglected in the momentum equation. The paper focuses on the case of neutral stability conditions, thus no additional terms concerning buoyancy effects and rotational effects are considered.

The numerical setup is classical and has been used for many applications and model assessments (e.g. [30, 3]). The simulated ABL is horizontally homogeneous. The horizontal directions are discretized pseudo-spectrally, and vertical derivatives are approximated with second-order central differences. The grid planes are staggered in the vertical with the first vertical velocity plane at a distance $\Delta z = H/(N_z - 1)$ from the surface, and the first horizontal velocity plane $\Delta z/2$ from the surface. The height of the computational domain is $H = 1000$m, and

the horizontal dimensions of the simulated volume are $L_x = L_y = 2\pi H$ . The domain is divided into $N_x$, $N_y$, and $N_z$ uniformly spaced grid points. We carried out simulations with resolutions of $N_x \times N_y \times N_z = 24 \times 24 \times 24$, $32 \times 32 \times 32$, $48 \times 48 \times 48$, $64 \times 64 \times 64$, $96 \times 96 \times 96$ and $128 \times 128 \times 128$. The filter width is computed using the common formulation $\widetilde{\Delta} = (\Delta x\, \Delta y\, \Delta z)^{1/3}$, where $\Delta x = L_x/N_x$ and $\Delta y = L_y/N_y$. The corresponding aliasing errors are corrected in the nonlinear terms according to the 3/2 rule [34]. The time advancement is carried out using a second-order-accurate Adams-Bashforth scheme [34]. All simulations have reached their statistically steady state.

The upper boundary conditions are $\frac{\partial \widetilde{u}_1}{\partial z} = 0$, $\frac{\partial \widetilde{u}_2}{\partial z} = 0$, and $\widetilde{u}_3 = 0$. At the bottom surface, the instantaneous wall stress is related to the velocity at the first vertical node through the application of the Monin-Obukhov similarity theory [35]. Although this theory was developed for mean quantities, it is common practice [6] in LES of atmospheric flows to use it for instantaneous fields as follows

$$\tau_{i3}|_w = -u_*^2 \frac{\widetilde{u}_i}{U(z)} = -\left(\frac{U(z)\,\kappa}{\ln(z/z_0) - \Psi_M}\right)^2 \frac{\widetilde{u}_i}{U(z)} \qquad (i = 1,\ 2)\ , \tag{7}$$

where $\tau_{i3}|_w$ is the instantaneous local wall stress, $u_*$ is the friction velocity, $z_0$ is the roughness length, $\kappa$ is the von Kármán constant, $\Psi_M$ is the stability correction for momentum, and $U(z)$ is the plane averaged resolved horizontal velocity. We adopt $\kappa = 0.4$ in this paper. In the literature, there are some variations on this value but generally they are within 5%. We take $u_* = 0.45\text{ms}^{-1}$ and $z_0 = 0.1\text{m}$, which is a similar setup as some previous studies [1, 29, 3]. In the case of neutral stability, $\Psi_M = 0$. The instantaneous resolved horizontal velocity is computed at a height of $z = \Delta z/2$. We use this classical scheme in order not to confuse effects with the SGS modeling which is the focus of the present work. Further, to reduce the error incurred by using a finite-difference approach to compute the vertical derivative of the nonlinear convective term $\widetilde{u}_3 \partial \widetilde{u}_1/\partial z$, we have employed a correction factor [3] at the bottom layer. This correction only improves the mean velocity profile in the lower levels, and appears to have no effect on other statistics.

# 4 Results and discussion

A series of large-eddy simulations with varying grid resolutions has been carried out using the baseline model, as well as the corrected model. For simplicity, 'simulation using the baseline model' is abbreviated to 'baseline simulation,' and 'simulation using the correct model' is abbreviated to 'corrected simulation.' Mean and turbulent statistics are gathered after statistically steady states were reached. In some subsections, we take the $64 \times 64 \times 64$-nodes simulation and the $128 \times 128 \times 128$-nodes simulation as base cases to present results. Also, we adopt the most commonly used symbols ($u$, $v$ and $w$) for the three velocity components.

## 4.1 Comparison with similarity theory predictions

In fluid dynamics, the log-law, which was first published by Theodore von Kármán [36], states that the mean streamwise velocity at a certain point in a turbulent boundary layer is proportional to the logarithm of the distance from that point to the wall. It is a self similar solution for the mean velocity parallel to the wall. The theory has been experimentally confirmed in a number of field experiments such as the Kansas experiment [35] and represents one of the most firmly established results against which new SGS models should be compared. For high-Reynolds-numbers boundary layer flows, where viscous effects can be negligible, it can be written as $< \widetilde{u} >= \frac{u_*}{\kappa} \ln\left(\frac{z}{z_0}\right)$, where $< \cdot >$ represents time and horizontal averaging in our study. The aerodynamic roughness, $z_0$, is necessarily nonzero since the log-law does not apply to the viscous sublayer.

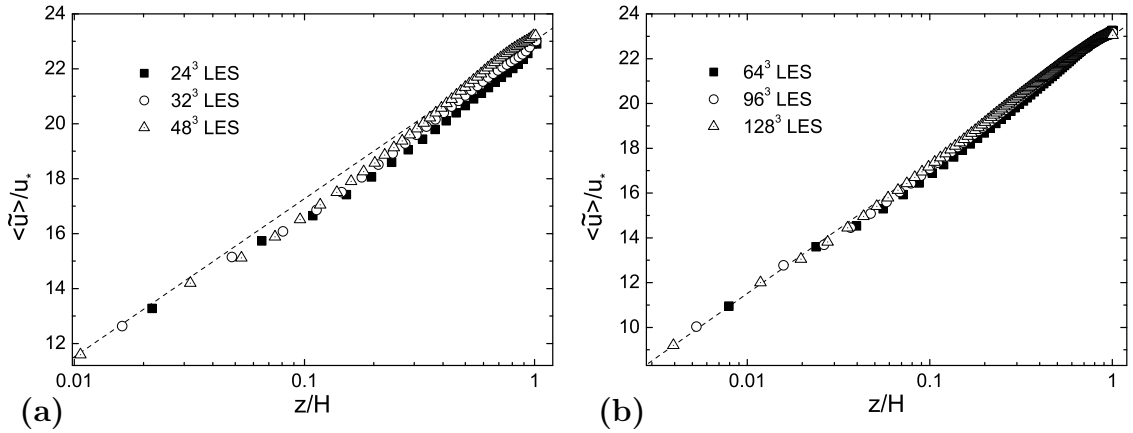


Figure 1: Normalized mean streamwise velocity profile in a semi-logarithmic scale: (a) results from low-resolution baseline simulations; (b) results from high-resolution baseline simulations. The dashed line corresponds to the classical log-law with $\kappa = 0.4$.

Though the log-law is a good approximation for the velocity profile of boundary layer turbulence, it is only technically applicable to the so-called surface layer, which occupies the lowest $10\% - 20\%$ of the flow in the atmospheric boundary layer. The mean streamwise velocity profile from different resolution baseline simulations and corrected simulations are presented in figure 1 and figure 2. Clearly, the mean streamwise velocity results are close to the expected log-law profile (straight dashed line). In the near-wall region, corrected simulations yield $< \widetilde{u} >$ closer to the log-law, compared with baseline simulations. Table 1 presents relative errors of $< \widetilde{u} >$ at a height of $z/H = 0.1$. All simulations yield small discrepancies with the log-law (relative errors within 5%). Baseline simulations have a tendency of increasing accuracy with increasing resolution. For the $96^3$ case and the $128^3$ case, corrected simulations yield slightly larger error magnitudes. This may be caused by the combined effects of the bottom boundary condition and the SGS modeling.

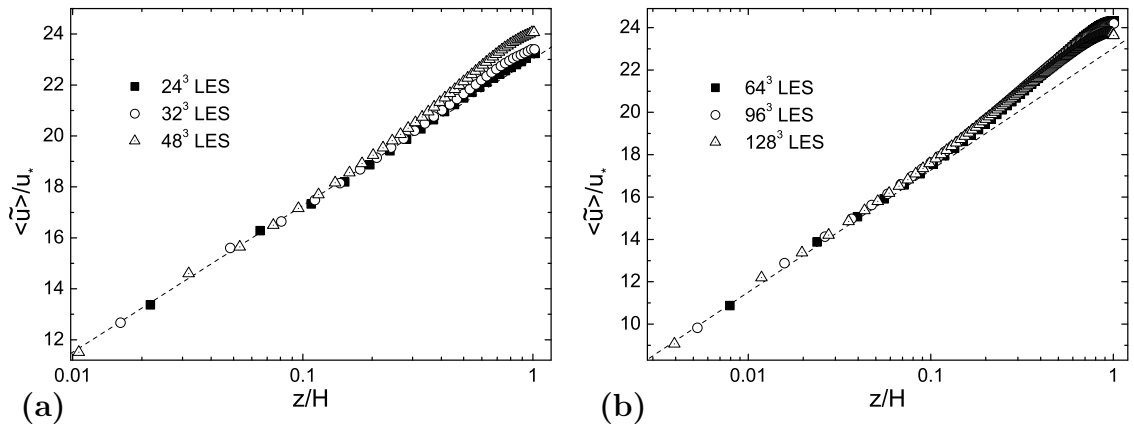


Figure 2: Normalized mean streamwise velocity profile in a semi-logarithmic scale: (a) results from low-resolution corrected simulations; (b) results from high-resolution corrected simulations. The dashed line corresponds to the classical log-law with $\kappa = 0.4$.

However, corrected simulations consistently show smaller discrepancies and weaker resolution dependence.

Table 1: Relative error of the mean streamwise velocity at a height of $z/H = 0.1$. $E = (u_{log} - < \widetilde{u} >)/u_{log}$, where $u_{log} = \frac{u_*}{\kappa} \ln\left(\frac{z}{z_0}\right)$.

| | $24^3$ LES | $32^3$ LES | $48^3$ LES | $64^3$ LES | $96^3$ LES | $128^3$ LES |
|---|---|---|---|---|---|---|
| $E$ from baseline simulations | 4.7% | 4.2% | 3.6% | 2.7% | 1.1% | 0.24% |
| $E$ from corrected simulations | 0.84% | 0.50% | 0.21% | −1.0% | −2.1% | −2.1% |

To more rigorously evaluate model performance, one may examine the values of the mean nondimensional vertical gradient of the streamwise velocity $\Phi = \frac{\kappa z}{u_*} \frac{d < \widetilde{u} >}{d z}$ as a function of vertical position. Theoretically, this nondimensional vertical gradient is unity in the surface layer. In 1994, Andrén et al. [1] performed an extensive comparison of various LES codes using the standard Smagorinsky model [37] with wall damping and other eddy-viscosity models. In the surface layer, from $z/H = 0$ to $z/H = 0.2$, their values of $\Phi$ were mostly larger than 1.2, and some simulations yielded $\Phi \approx 2$. Similar overshoots in $\Phi$ reaching over 1.5 for the standard Smagorinsky model have been observed in many studies [38, 39, 40, 4]. It appears that the standard Smagorinsky model is too dissipative, removing too much kinetic energy from the resolved field and generating a near-linear profile in the surface layer, which bears a large value of $\Phi$. The values of $\Phi$ resulting from the present simulations are presented in figure 3 and figure 4. The modulated gradient model yields a value of $\Phi$ that remains close to 1 in the surface layer, indicative of the expected logarithmic ve-

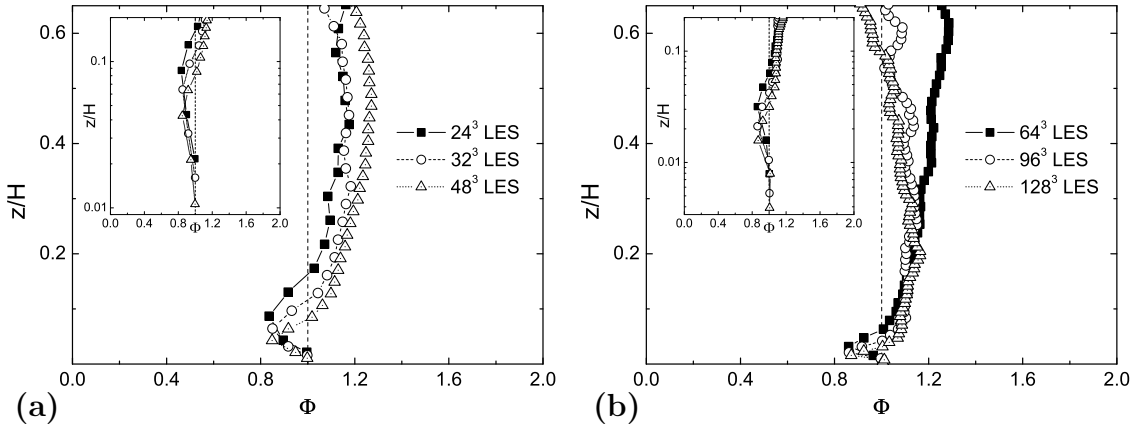


Figure 3: Nondimensional vertical gradient of the mean streamwise velocity ($\Phi = \frac{\kappa z}{u_*}\frac{d<\widetilde{u}>}{dz}$) versus normalized height above the wall: (a) results from low-resolution baseline simulations; (b) results from high-resolution baseline simulations. The dashed line corresponds to the classical log-law with $\kappa = 0.4$. The left corner plot is a zoomed view of the near-wall region and it has a log scale in the vertical direction.

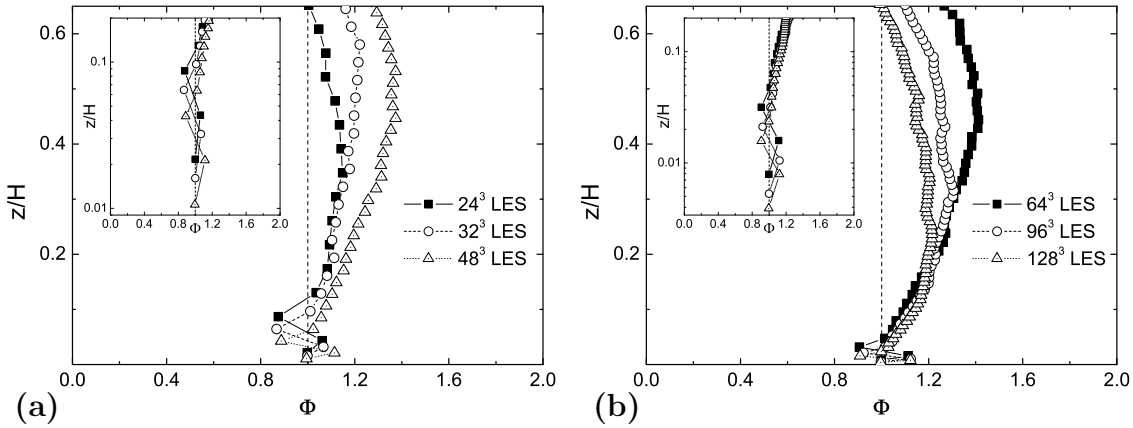


Figure 4: Nondimensional vertical gradient of the mean streamwise velocity ($\Phi = \frac{\kappa z}{u_*}\frac{d<\widetilde{u}>}{dz}$) versus normalized height above the wall: (a) results from low-resolution corrected simulations; (b) results from high-resolution corrected simulations. The dashed line corresponds to the classical log-law with $\kappa = 0.4$. The left corner plot is a zoomed view of the near-wall region and it has a log scale in the vertical direction.

locity profile. It should be noted that using the baseline model, the nondimensional vertical gradient is slightly underestimated for the lowest 2-3 grid points (with the lowest value of about 0.85), which leads to the slight underestimation of the average velocity as shown in figure 1 and table 1. The corrected model appears to remove this bias.

Next, figure 5 shows the vertical distribution of the averaged value of the correction coefficient computed using equation (4) for different resolution simulations.

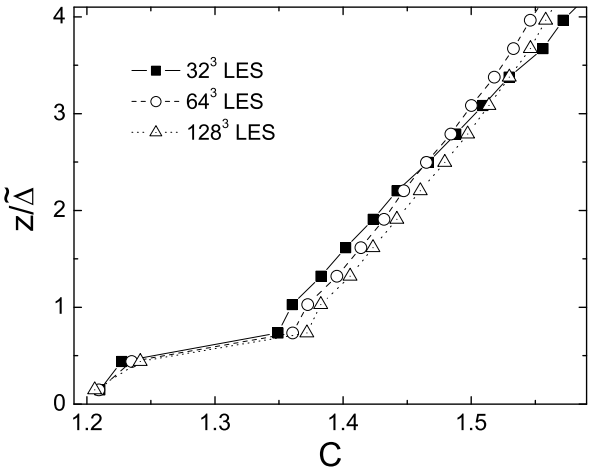


Figure 5: Vertical distribution of the time-averaged correction coefficient obtained from three corrected simulations. The height is normalized with the filer size $\widetilde{\Delta}$.

The value of $C$ is larger than 1 due to the fact that the denominator in equation (4) is always smaller than the numerator, since all negative values of the SGS energy transfer rate have been clipped to zero. This correction compensates for the overestimation of the SGS energy transfer rate associated with the use of the clipping procedure. $C$ has values that increase with height and range from about 1.2 near the surface to 1.6 away from the surface. Note that the collapse of all curves indicates that the value of $C$ is dependent on $z/\widetilde{\Delta}$ only.

## 4.2 Energy spectra

It is important to test the ability of LES to accurately reproduce the main spectral characteristics of the resolved field. Spectra of velocity fields in turbulent boundary layers are known to exhibit three distinct spectral scaling regions: the energy-production range, the inertial subrange and the dissipation range. In the case of LES of high-Reynolds-number boundary layers, the dissipation range is not resolved and, therefore, it will not be considered here. It is well known [41, 42, 43] that the energy spectra of three wind components satisfy the Kolmogorov $-5/3$ power-law in the inertial subrange, i.e., the range of relatively small, isotropic scales that satisfy $k_1 z \gtrsim 1$, where $k_1$ is the streamwise wavenumber. Also, laboratory and field measurements [41, 43, 44] of boundary-layer turbulence show that in the energy-production range, corresponding to scales larger than the distance to the surface ($k_1 z \lesssim 1$) and smaller than the integral scale, spectra of the streamwise velocity often follow a $-1$ power-law, i.e., they are proportional to $k_1^{-1}$.

Previous LES studies have examined model performance regarding energy spectra, and limitations have been found for traditional SGS models. The spectra of the streamwise velocity obtained using the standard Smagorinsky model decay sig-

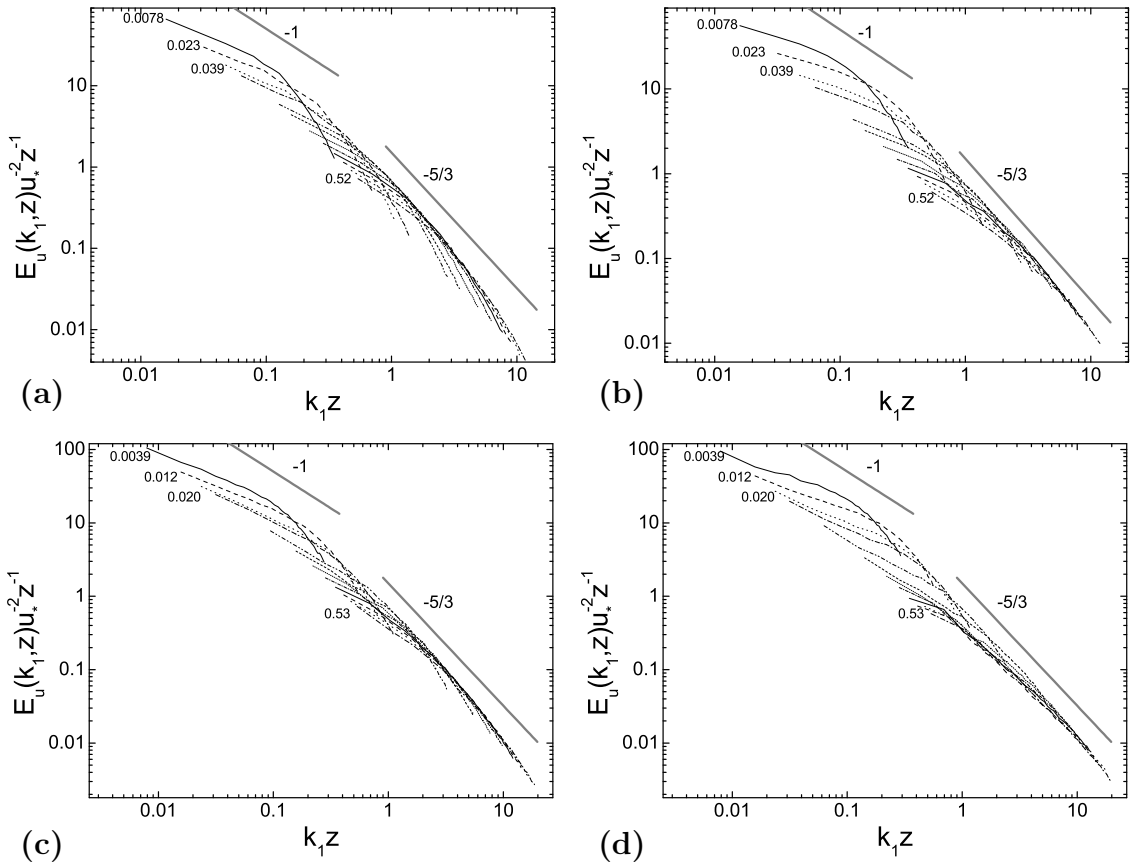


Figure 6: Averaged nondimensional 1-D spectra of the streamwise velocity obtained from (a) the $64^3$ baseline simulation; (b) the $64^3$ corrected simulation; (c) the $128^3$ baseline simulation; and (d) the $128^3$ corrected simulation. Numbers in plots denote normalized heights ($z/H$). The slopes of $-1$ and $-5/3$ are also shown.

nificantly faster (some simulations yield spectrum slopes as large as $-7$) than the expected $-1$ power-law in the near-wall region [1, 40, 3]. Within the constraints of the Smagorinsky model, this type of spectrum means that the model dissipates kinetic energy at an excessive rate. The resulting spectra obtained using the dynamic Smagorinsky model, on the other hand, decay too slowly (the spectrum slope is close to $-0.5$) in the near-wall region [3]. This is likely to be due to the fact that the dynamic procedure samples scales near and beyond the local integral scale, at which the assumption of scale invariance of the coefficient (on which the model relies) breaks down, leading to an underestimation of the Smagorinsky coefficient near the surface [3]. The lower coefficient then yields lower energy dissipation rate and pile-up of energy at high wavenumbers. It is also found that, in the inertial subrange, the dynamic Smagorinsky model may yield a streamwise velocity spectrum slope shallower (close to $-0.8$) than $-5/3$ [7].

Figure 6 and figure 7 show the normalized spectra of the simulated streamwise

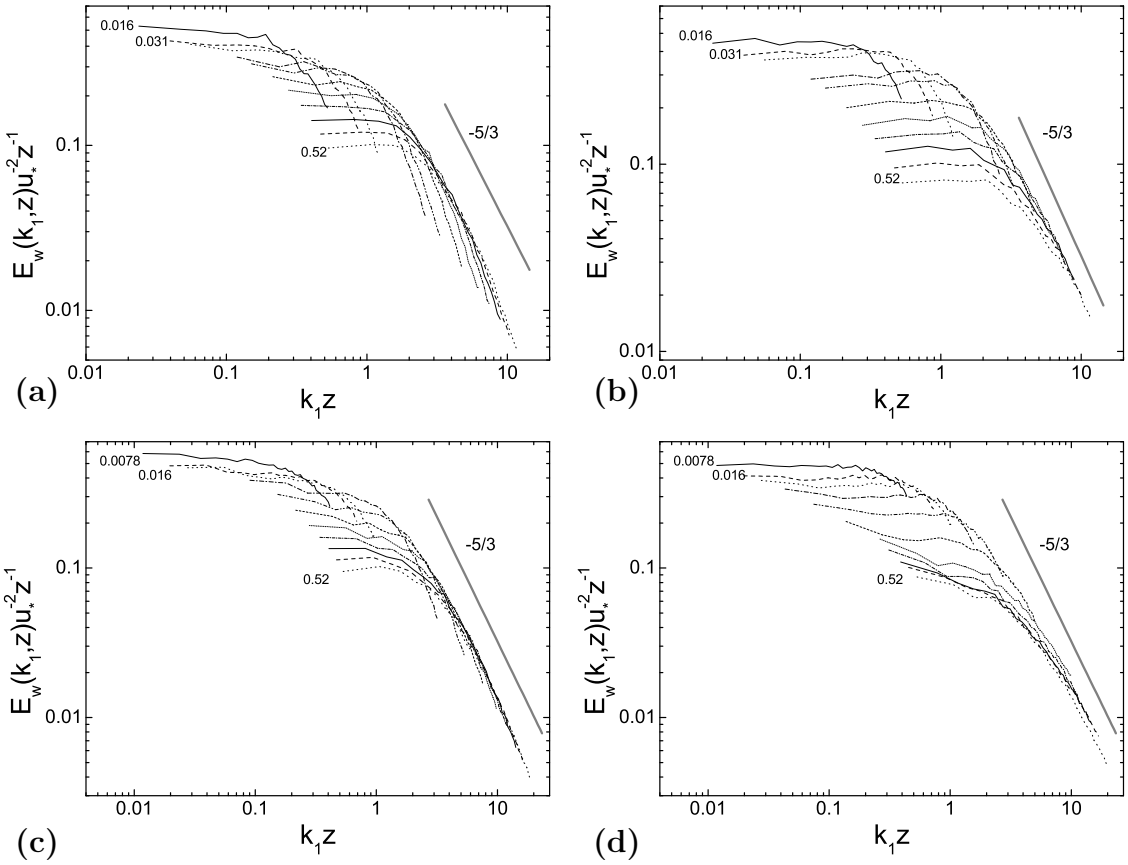


Figure 7: Averaged nondimensional 1-D spectra of the vertical velocity obtained from (a) the $64^3$ baseline simulation; (b) the $64^3$ corrected simulation; (c) the $128^3$ baseline simulation; and (d) the $128^3$ corrected simulation. Numbers in plots denote normalized heights ($z/H$). The slope of $-5/3$ is also shown.

and vertical velocity, computed at different heights. Results are presented for the two model versions (with the baseline simulation results on the left panels, and with the corrected simulation results on the right panels) as well as two different resolutions (the $64^3$ resolution results on the top panels, and the $128^3$ resolution results on the bottom panels). Spectra are calculated from one-dimensional Fourier transforms of the velocity component and then are averaged both horizontally and in time. Streamwise wavenumber is normalized by the height, and spectrum magnitude is normalized by $u_*^2 z$. It should be noted that the spectra of the spanwise velocity (not shown here) are similar to the spectra of the streamwise velocity. The baseline model leads to spectra that are consistently too steep at large wavenumbers. This is consistent with the feature that the baseline model overestimates the dissipation rate. This excessive dissipation is more evident in the coarser resolution ($64^3$-nodes baseline simulation). Results are clearly improved for both resolutions when the correction given by equation (4) is used. In that case, in the inertial subrange ($k_1 z \gtrsim 1$) all the normalized spectra show a better collapse and are in good agreement with

the $-5/3$ power-law. The improvement in the dissipation characteristics of the model due to the correction can be explained considering that the relatively larger values of $C$ (see figure 5) provided by the correction lead to relatively smaller values of $\tau_{ij}$ and, consequently, SGS energy transfer rates. For scales larger than the distance to the surface ($k_1 z \lesssim 1$), the slope of the spectra of the streamwise velocity is slightly lower than $-1$ (close to $-0.7$). The spectra of the vertical velocity differ from the spectra of the streamwise velocity. As shown in figure 7, there is no clear $-1$ power-law region; instead the spectra are flat in the near-wall region. This finding is consistent with the expected distribution supported by theoretical [45, 41] and experimental studies [41, 43].

## 4.3 Flow visualization

A few remarks must be made regarding the ability of LES calculations to capture the structure of turbulence. We define three components of the resolved velocity fluctuation as $\widetilde{u}_i' = \widetilde{u}_i - < \widetilde{u}_i >$. Coherent streamwise elongated 'streaks' of $\widetilde{u}'$ are ubiquitous in turbulent boundary flows and have been repeatedly observed in a variety of contexts [46, 47, 48]. Figures 8(a, c, e) present instantaneous contours of $\widetilde{u}'/u_*$ on a horizontal plane obtained from the $64^3$ baseline simulation, the $128^3$ baseline simulation and the $128^3$ corrected simulation respectively. Elongated structures of high-speed and low-speed $\widetilde{u}'$ are evident. The contours of $\widetilde{u}'/u_*$ are more diffused in the $64^3$ baseline simulation. As expected, the $128^3$ baseline simulation shows finer structures. This observation is consistent with other LES studies of turbulent boundary flows [7, 40]. Low-speed streak-like structure is closely related to vortical motions and corresponds to streamwise momentum being transported away from the wall. Figures 8(c, e) show that the low-speed regions appear more concentrated and elongated (often spanning the entire streamwise domain in our simulations) than the high-speed regions. This finding is consistent with LES and DNS results [49, 12, 48, 50] and recent experimental measurements [47, 48]. Moreover, figures 8(c ,e) reveal a clear difference between the structure of the streaks simulated with both models under consideration. Using the correction coefficient yields simulated streamwise velocity fields that have more small-scale structure. This is consistent with the fact that the baseline model dissipates too much energy (as pointed in the energy spectra subsection), thus overly smoothing the velocity fields at the smallest resolved scales.

Figures 8(b, d, f) present instantaneous contours of $\widetilde{w}'/u_*$ on a vertical plane obtained from the $64^3$ baseline simulation, the $128^3$ baseline simulation and the $128^3$ corrected simulation respectively. The strong vertical coherence of the updrafts and downdrafts is evident. Small plumes originate near the ground, and some of them are suppressed by strong downdrafts, while others merge with their neighbors to form larger stronger updrafts. The updraft regions are stronger and more spatially coherent than the downdraft regions, and also the near-wall low-speed streaks (as shown in Fig. 8(a, c, e) ) are kinematically tied to the presence of strong updrafts.

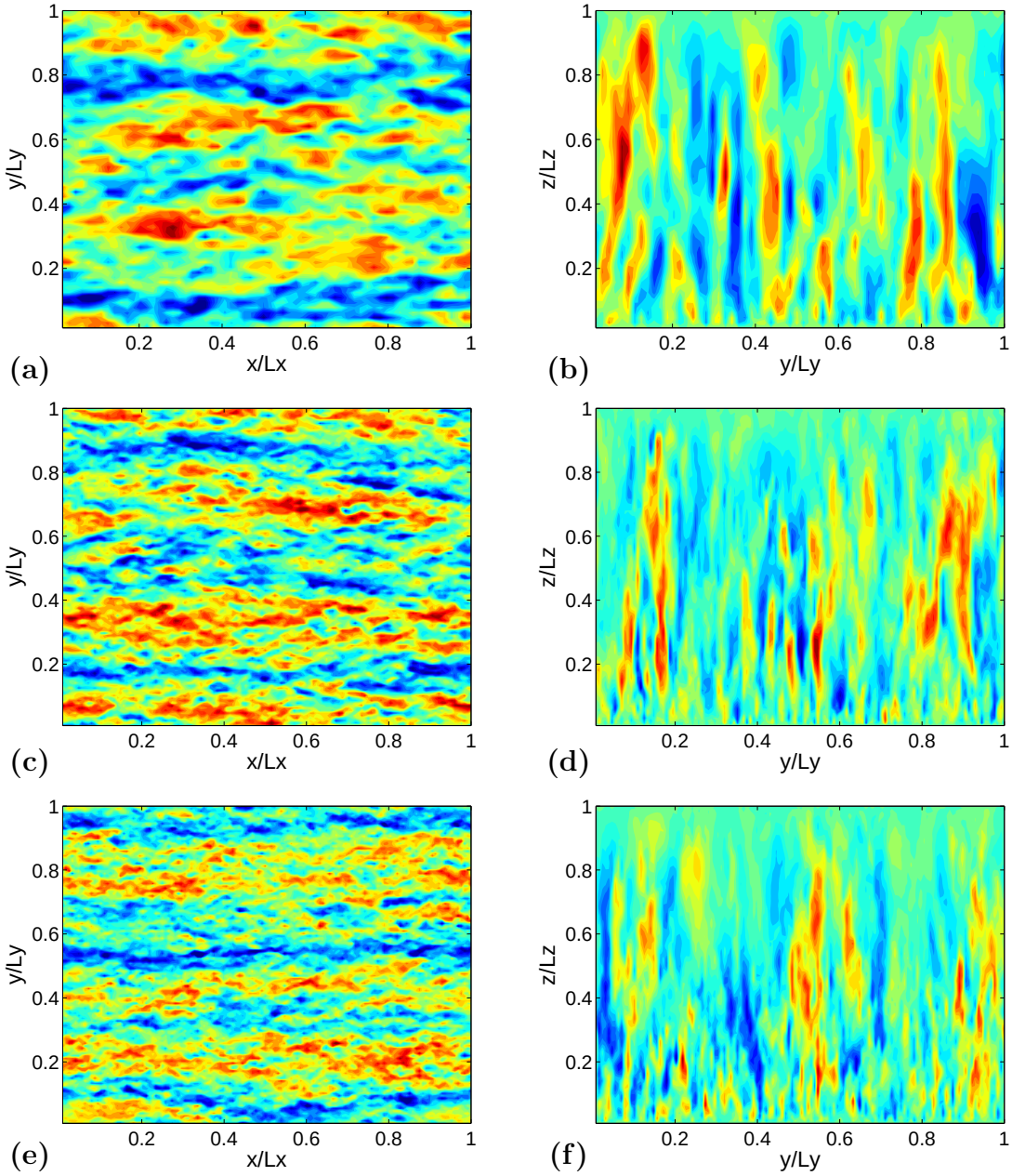


Figure 8: Instantaneous velocity fluctuation contours: (a, c, e) $\widetilde{u}'/u_*$ at a height of $z/H = 0.1$ obtained from the $64^3$ baseline simulation, the $128^3$ baseline simulation and the $128^3$ corrected simulation; and (b, d, f) $\widetilde{w}'/u_*$ in the layer of $x/L_x = 0.5$ obtained from the $64^3$ baseline simulation, the $128^3$ baseline simulation and the $128^3$ corrected simulation. Each plot adopts a 25 contour-level linear scale color-map, which uses blue to represent $\widetilde{u}'/u_* = -6$ and $\widetilde{w}'/u_* = -3$, and uses red to represent $\widetilde{u}'/u_* = 6$ and $\widetilde{w}'/u_* = 3$.

These turbulent structures are consistent with results in other studies [49, 12]. Like in the case of the horizontal velocity fields, using the correction coefficient yields simulated vertical velocity fields that have more small-scale structure.

## 4.4 PDF of velocity fluctuations

Based on the central limit theorem, probability density functions (PDF) for turbulent velocities are near-Gaussian. Experimental studies [51, 52] have confirmed this statement in turbulent boundary layer flows, particularly near the wall. Figure 9 examines the PDF of $\widetilde{u}'/u_*$, $\widetilde{v}'/u_*$ and $\widetilde{w}'/u_*$ at a height of $z/H = 0.1$ obtained from simulations using the two model versions at two resolutions. To accentuate the PDF tails, a log ordinate axis is used. PDF plots are very weakly skewed, and the approach to Gaussian distribution is evident.

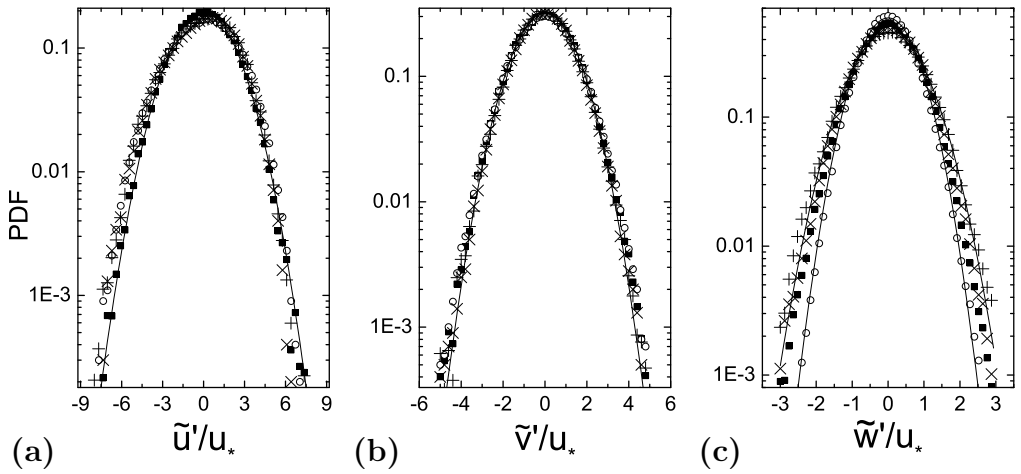


Figure 9: Probability density functions of resolved velocity fluctuations at a height of $z/H = 0.1$ obtained from ■: the $64^3$ corrected simulation; ◯: the $64^3$ baseline simulation; +: the $128^3$ corrected simulation; and ×: the $128^3$ baseline simulation. The solid lines are zero-skewness Gaussian curves.

To quantitatively examine their statistical characteristics, the skewness and flatness (also referred to as 'kurtosis') factors are shown in figure 10 and figure 11. The magnitude of skewness factors is generally smaller than 0.5, indicating a weakly skewed ($|S| < 1.5$) probability distribution. As required by the spanwise symmetry of the flow, the skewness of $\widetilde{v}'$ must be nearly zero, and current simulations demonstrate this symmetry reasonably well as seen in figure 10(b). The skewness of $\widetilde{u}'$, as revealed through previous experiments [51] and LES studies [7, 12], is mostly negative indicating a predominance of negative streamwise velocity fluctuations accompanying more elongated low-speed streaks as shown in figures 8(a, c, e). Also, consistent with previous studies [51], the flatness factors of the three fluctuating velocity components are close to the value of 3 which Gaussian distribution bears.

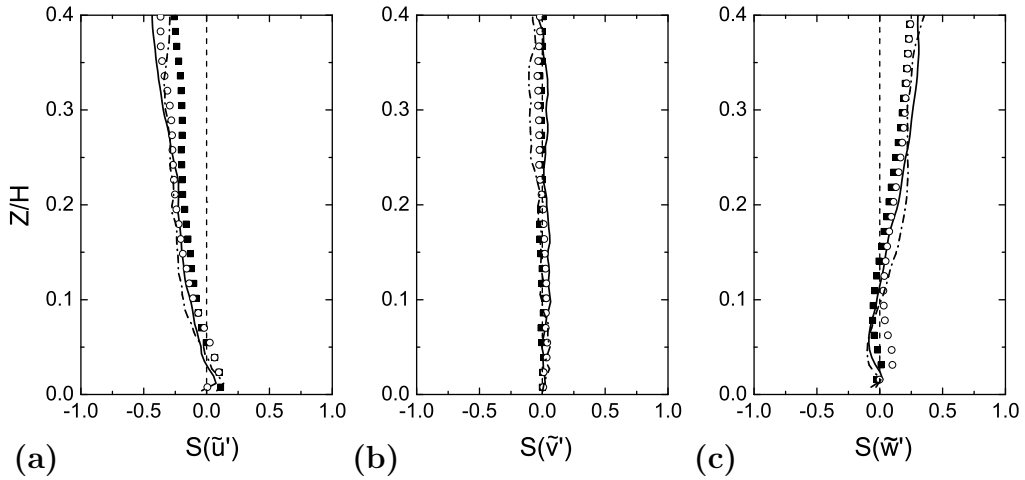


Figure 10: Vertical distribution of skewness factor of resolved velocity fluctuations obtained from ■: the $64^3$ corrected simulation; ◯: the $64^3$ baseline simulation; dash dotted line: the $128^3$ corrected simulation; and solid line: the $128^3$ baseline simulation.

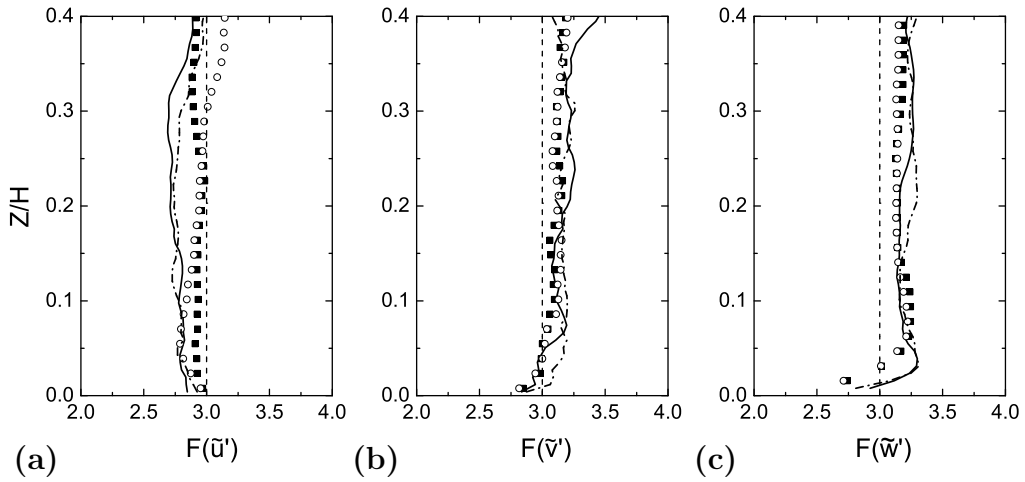


Figure 11: Vertical distribution of flatness factor of resolved velocity fluctuations obtained from ■: the $64^3$ corrected simulation; ◯: the $64^3$ baseline simulation; dash dotted line: the $128^3$ corrected simulation; and solid line: the $128^3$ baseline simulation.

## 4.5 Second-order moment statistics

Averaging (both horizontally and in time) the streamwise direction momentum equation yields $\frac{\partial <\widetilde{u}\,\widetilde{w}>}{\partial z} + \frac{\partial <\tau_{xz}>}{\partial z} = -\frac{\partial <\widetilde{p}>}{\partial x}$, where $<\widetilde{u}\,\widetilde{w}>$ is the mean resolved shear stress and $<\tau_{xz}>$ is the mean SGS shear stress. Since the simulated flow is driven by a constant pressure gradient, in the absence of viscous stresses, the normalized (by $u_*^2$) mean total turbulent stress grows linearly from a value of $-1$ at the surface

to a value of 0 at the top of the boundary layer. Because $< \widetilde{w} >= 0$, it is easy to prove that $< \widetilde{u}\,\widetilde{w} >$ equals $< \widetilde{u}'\,\widetilde{w}' >$. Mean resolved shear stress should be negative indicating an overall tendency that faster ($\widetilde{u}' > 0$) fluid parcels moving downward ($\widetilde{w}' < 0$) and slower ($\widetilde{u}' < 0$) fluid parcels moving upward ($\widetilde{w}' > 0$). Figure 12 shows the vertical distribution of the mean total and partial (resolved and subgrid-scale) values of the normalized shear stress obtained from the $128^3$ baseline simulation and the normalized SGS stresses obtained from two coarser grids ($64^3$ and $96^3$). As expected, the coarser resolution simulations yield SGS stresses that are larger in magnitude than the higher resolution counterparts. The distribution of total turbulent stress is indeed consistent with the expected linear behavior. The result also serves as a confirmation of stationarity and momentum conservation of the scheme.

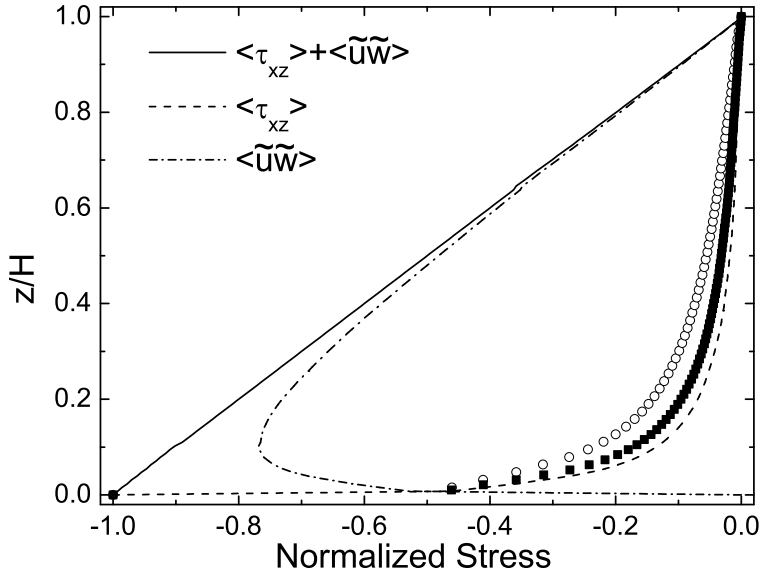


Figure 12: Vertical distribution of normalized (by $u_*^2$) total and partial (subgrid-scale and resolved) shear stresses. Lines represent results obtained from the $128^3$ baseline simulation, respectively, solid line: total stress; dashed line: SGS stress; and dash dotted line: resolved stress. Also shows ■: SGS stress from the $96^3$ baseline simulation; ◯: SGS stress from the $64^3$ baseline simulation.

Figure 13 shows the vertical distribution of the variance of the resolved velocities. The current simulation results are in good agreement with the scale-dependent dynamic model results in Porté-Agel et al.'s past work [3], which used the same numerical setup. Also, the agreement between the results from different resolution simulations is good for the two horizontal velocity components. Differences can be observed between vertical velocity variances obtained from different resolution simulations: higher resolution simulations yield higher maximum $< \widetilde{w}'\widetilde{w}' >$ values, and lower elevation where the maximum $< \widetilde{w}'\widetilde{w}' >$ occurs. This resolution dependence is

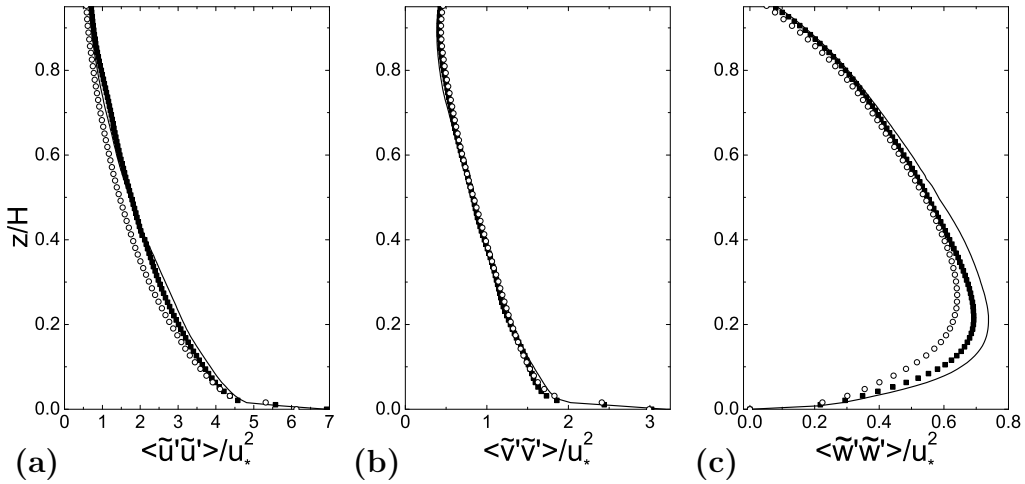


Figure 13: Vertical distribution of normalized variances of the resolved velocities obtained from solid line: $128^3$ baseline simulation; ■: $96^3$ baseline simulation; and ◯: $64^3$ baseline simulation.

due to the fact that, near the surface, the SGS vertical velocity variance represents a relatively large fraction of the total vertical velocity variance as seen in figure 7. As a result, an increase in resolution leads to a smaller SGS vertical velocity variance and, in turn, a larger resolved vertical velocity variance. This contrasts with the behavior of the horizontal velocity variance, which is dominated by larger (resolved in LES) horizontal eddy scales (see also figure 6) and, consequently, shows little dependence on resolution.

# 5 Summary and conclusions

We have proposed a new nonlinear SGS model and tested it in simulations of a neutrally stratified ABL turbulence. The model uses the SGS kinetic energy to compute the magnitude of the SGS stress tensor, and the gradient tensor (which can be derived by Taylor expansion of the SGS stress) to determine its structure, i.e, the relative magnitude of the different tensor components. Different from standard gradient models, the formulation of the new model is derived from a class of one-equation models, which was introduced recently [24, 11]. Here, we use the local equilibrium hypothesis to estimate the SGS kinetic energy, and adopt a clipping procedure to avoid local kinetic energy transfer from unresolved to resolved scales. This, together with the fact that the model only uses local velocity gradients, and it does not require an extra filtering, make this model computationally efficient. Two approaches are considered to specify the model coefficient: a constant value of 1, and a simple correction to account for the effects of the clipping procedure on the SGS production rate.

The proposed model is examined in simulations of the well-established case of

a neutral ABL flow. These simulations are the first successful calculations of ABL turbulence using an unmixed gradient scheme. In summary, the basic conclusions from this paper are: (i) the standard gradient model can be modified to achieve stable and robust simulations; (ii) the local equilibrium hypothesis together with clipping procedure may provide an estimation of the SGS kinetic energy for the model; (iii) application to a neutral ABL flow shows the model is capable to achieve the expected logarithmic velocity profile in the near-wall region, the correct spectral scaling, as well as some other important statistical characteristics of boundary layer turbulence.

It is well known that LES of the ABL is rather sensitive to the SGS model in the near-wall region. This is due to the fact that the near-surface flow is highly anisotropic and the SGS motions account for a large fraction of the turbulence, as shown by the energy spectra of the different velocity components (Fig. 6 and 7). The proposed model shows a significant improvement with respect to other simple models, such as the standard Smagorinsky model, which is known to overestimate the nondimensional vertical gradient of the streamwise velocity near the surface [38, 1, 39, 40, 4] and it yields energy spectra that are too steep due to its overly dissipative nature [1, 40, 3].

The model is still lacking in that, in its present formulation, it needs *a-priori* knowledge to determine the model coefficient. It is important to note that the selected constant value is based on theoretical arguments, which are strictly only valid in the inertial subrange of high-Reynolds-number turbulence. However, the filter size usually falls outside of the inertial subrange in the near-wall region of ABL. Possible future modifications of the model include the development and testing of dynamic and scale-dependent dynamic procedures to optimize the value of the model coefficient using information of the resolved velocity field. Moreover, alternative ways of computing the SGS kinetic energy could be considered, including the solution of an additional transportation equation. *A-priori* studies using field data could also be used to test the new closure (equation (1)). Future work should also extend the implementation of a similar base model to SGS scalar fluxes.

# 6 Acknowledgment

This research was supported by the National Science Foundation (grants EAR-0537856 and ATM-0854766), NASA (grant NNG06GE256), customers of Xcel Energy through a grant (RD3-42) from the Renewable Development Fund, and the University of Minnesota Institute for Renewable Energy and the Environment. Computing resources were provided by the Minnesota Supercomputing Institute.

# References


[1] A. Andren, A. R. Brown, J. Graf, P. J. Mason, C.-H. Moeng, F. T. M. Nieuwstadt, and U. Schumann, "Large-eddy simulation of a neutrally stratified boundary layer: a comparison of four computer codes," *Q. J. R. Meteorol. Soc.*, vol. 120, no. 520, pp. 1457–1484, 1994.

[2] S. Khanna and J. G. Brasseur, "Analysis of monin?obukhov similarity from large-eddy simulation," *J. Fluid Mech.*, vol. 345, pp. 251–286, 1997.

[3] F. Porté-Agel, C. Meneveau, and M. B. Parlange, "A scale-dependent dynamic model for large-eddy simulation: application to a neutral atmospheric boundary layer," *J. Fluid Mech.*, vol. 415, pp. 261–284, 2000.

[4] F. K. Chow, R. L. Street, M. Xue, and J. H. Ferziger, "Explicit filtering and reconstruction turbulence modeling for large-eddy simulation of neutral boundary layer flow," *J. Atmos. Sci.*, vol. 62, pp. 2058–2077, 2005.

[5] J. W. Deardorff, "The use of subgrid transport equations in a three-dimensional model of atmospheric turbulence," *J. Fluids Eng.*, vol. 95, pp. 429–438, 1973.

[6] C.-H. Moeng, "A large-eddy-simulation model for the study of planetary boundary-layer turbulence," *J. Atmos. Sci.*, vol. 41, pp. 2052–2062, 1984.

[7] U. Piomelli, "High Reynolds number calculations using the dynamic subgrid-scale stress model," *Phys. Fluids*, vol. 5, pp. 1484–1490, June 1993.

[8] S. Liu, C. Meneveau, and J. Katz, "On the properties of similarity subgrid-scale models as deduced from measurements in a turbulent jet," *J. Fluid Mech.*, vol. 275, pp. 83–119, 1994.

[9] C. W. Higgins, M. B. Parlange, and C. Meneveau, "Alignment trends of velocity gradients and subgrid-scale fluxes in the turbulent atmospheric boundary layer," *Boundary Layer Meteorol.*, vol. 109, pp. 59–83, 2003.

[10] S. Menon, P.-K. Yeung, and W.-W. Kim, "Effect of subgrid models on the computed interscale energy transfer in isotropic turbulence," *Comp. Fluids*, vol. 25, no. 2, pp. 165–180, 1996.

[11] H. Lu, C. J. Rutland, and L. M. Smith, "A-priori tests of one-equation LES modeling of rotating turbulence," *J. Turbul.*, vol. 8, no. 37, pp. 1–27, 2007.

[12] S. Khanna and J. G. Brasseur, "Three-dimensional buoyancy- and shear-induced local structure of the atmospheric boundary layer," *J. Atmos. Sci.*, vol. 55, pp. 710–743, 1998.

[13] A. Juneja and J. G. Brasseur, "Characteristics of subgrid-resolved-scale dynamics in anisotropic turbulence, with application to rough-wall boundary layers," *Phys. Fluids*, vol. 11, no. 10, pp. 3054–3068, 1999.

[14] H. Kobayashi and Y. Shimomura, "The performance of dynamic subgrid-scale models in the large eddy simulation of rotating homogeneous turbulence," *Phys. Fluids*, vol. 13, pp. 2350–2360, August 2001.

[15] K. Horiuti, "Transformation properties of dynamic subgrid-sale models in a frame of reference undergoing rotation," *J. Turbul.*, vol. 7, no. 16, pp. 1–27, 2006.

[16] H. Lu, C. J. Rutland, and L. M. Smith, "A posteriori tests of one-equation LES modeling of rotating turbulence," *Int. J. Mod. Phys. C*, vol. 19, pp. 1949–1964, 2008.

[17] C. Cambon, N. N. Mansour, and F. S. Godeferd, "Energy transfer in rotating turbulence," *J. Fluid Mech.*, vol. 337, pp. 303–332, 1997.

[18] L. M. Smith and F. Waleffe, "Transfer of energy to two-dimensional large scales in forced, rotating three-dimensional turbulence," *Phys. Fluids*, vol. 11, pp. 1608–1622, June 1999.

[19] R. A. Clark, J. H. Ferziger, and W. C. Reynolds, "Evaluation of subgrid-scale models using an accurately simulated turbulent flow," *J. Fluid Mech.*, vol. 91, no. 1, pp. 1–16, 1979.

[20] C. Meneveau and J. Katz, "Scale-invariance and turbulence models for large-eddy simulation," *Annu. Rev. Fluid Mech.*, vol. 32, pp. 1–32, 2000.

[21] P. Sagaut, *Large eddy simulation for incompressible flows*. Springer-Verlag, Berlin Heidelberg, 3rd ed., 2006.

[22] J. Bardina, J. H. Ferziger, and W. C. Reynolds, "Improved subgrid scale models for large eddy simulation," *AIAA Paper 80-1357*, 1980.

[23] B. Vreman, B. Geurts, and H. Kuerten, "Large-eddy simulation of the turbulent mixing layer," *J. Fluid Mech.*, vol. 339, pp. 357–390, 1997.

[24] E. Pomraning and C. J. Rutland, "Dynamic one-equation nonviscosity large-eddy simulation model," *AIAA Journal*, vol. 40, pp. 689–701, April 2002.

[25] M. Germano, U. Piomelli, and W. H. Cabot, "A dynamic subgrid-scale eddy viscosity model," *Phys. Fluids A*, vol. 3, pp. 1760–1765, July 1991.

[26] A. Yoshizawa and K. Horiuti, "A statistically-derived subgrid-scale kinetic energy model for the large-eddy simulation of turbulent flows," *J. Phys. Soc. Jpn.*, vol. 54, pp. 2834–2839, August 1985.

[27] W.-W. Kim and S. Menon, "A new dynamic one-equation subgrid-scale model for large eddy simulations," *AIAA Paper 1995-356*, 1995.

[28] S. B. Pope, *Turbulent flows*. Cambridge University Press, Cambridge, 2000.

[29] J. D. Albertson, *Large eddy simulation of land-atmosphere interaction*. PhD thesis, Univ. of California - Davis, 1996.

[30] J. D. Albertson and M. B. Parlange, "Natural integration of scalar fluxes from complex terrain," *Advan. Water Resour.*, vol. 23, pp. 239–252, 1999.

[31] F. Porté-Agel, "A scale-dependent dynamic model for scalar transport in large-eddy simulations of the atmospheric boundary layer," *Boundary Layer Meteorol.*, vol. 112, pp. 81–105, 2004.

[32] R. Stoll and F. Porté-Agel, "Effect of roughness on surface boundary conditions for large-eddy simulation," *Boundary Layer Meteorol.*, vol. 118, pp. 169–187, January 2006.

[33] F. Wan, F. Porté-Agel, and R. Stoll, "Evaluation of dynamic subgrid-scale models in large-eddy simulations of neutral turbulent flow over a two-dimensional sinusoidal hill," *Atmos. Env.*, vol. 41, no. 13, pp. 2719–2728, 2007.

[34] C. Canuto, M. Y. Hussaini, A. Quarteroni, and T. A. Zang, *Spectral methods in fluid dynamics*. Sprnger-Verlag, Berlin Heidelberg, 1988.

[35] J. A. Businger, J. C. Wynagaard, Y. Izumi, and E. F. Bradley, "Flux-profile relationships in the atmospheric surface layer," *J. Atmos. Sci.*, vol. 28, pp. 181–189, 1971.

[36] T. von Kármán, "Mechanical similitude and turbulence," *Tech. Mem., No. 611, Washington D.C., NACA*, 1931.

[37] J. Smagorinsky, "General circulation experiments with the primitive equations: I. the basic experiment," *Mon. Weather Rev.*, vol. 91, no. 3, pp. 99–164, 1963.

[38] P. J. Mason and D. J. Thomson, "Stochastic backscatter in large-eddy simulations of boundary layers," *J. Fluid Mech.*, vol. 242, pp. 51–78, 1992.

[39] P. E. Sullivan, J. C. Mcwilliams, and C.-H. Moeng, "A subgrid-scale model for large-eddy simulation of planetary boundary-layer flows," *Boundary Layer Meteorol.*, vol. 71, pp. 247–276, 1994.

[40] B. Kosović, "Subgrid-scale modelling for the large-eddy simulation of high-Reynolds-number boundary layers," *J. Fluid Mech.*, vol. 336, pp. 151–182, 1997.

[41] A. E. Perry, S. Henbest, and M. S. Chong, "A theoretical and experimental study of wall turbulence," *J. Fluid Mech.*, vol. 165, pp. 163–199, 1986.

[42] S. G. Saddoughi and S. V. Veeravalli, "Local isotropy in turbulent boundary layers at high Reynolds number," *J. Fluid Mech.*, vol. 268, pp. 333–372, 1994.

[43] G. G. Katul and C. R. Chu, "A theoretical and experimental investigation of energy-containing scales in the dynamic sublayer of boundary-layer flows," *Boundary Layer Meteorol.*, vol. 86, no. 2, pp. 279–312, 1998.

[44] G. J. Kunkel and I. Marusic, "Study of the near-wall-turbulent region of the high-Reynolds-number boundary layer using an atmospheric flow," *J. Fluid Mech.*, vol. 548, pp. 375–402, 2006.

[45] A. A. Townsend, *The structure of turbulent shear flow.* Cambridge University Press, 2nd ed., 1976.

[46] S. J. Kline, W. C. Reynolds, F. A. Schraub, and P. W. Runstadler, "The structure of turbulent boundary layers," *J. Fluid Mech.*, vol. 30, pp. 741–773, 1967.

[47] C. D. Tomkins and R. J. Adrian, "Spanwise structure and scale growth in turbulent boundary layers," *J. Fluid Mech.*, vol. 490, pp. 37–74, 2003.

[48] N. Hutchins and I. Marusic, "Evidence of very long meandering features in the logarithmic region of turbulent boundary layers," *J. Fluid Mech.*, vol. 579, pp. 1–28, 2007.

[49] C. H. Moeng and P. E. Sullivan, "A comparison of shear- and buoyancy-driven planetary boundary layer flows," *J. Atmos. Sci.*, vol. 51, no. 7, pp. 999–1022, 1994.

[50] X. Wu and P. Moin, "Direct numerical simulation of turbulence in a nominally zero-pressure-gradient flat-plate boundary layer," *J. Fluid Mech.*, vol. 630, pp. 5–41, July 2009.

[51] J.-L. Balint, J. M. Wallace, and P. Vukoslavčević, "The velocity and vorticity vector fields of a turbulent boundary layer. part 2. statistical properties," *J. Fluid Mech.*, vol. 228, pp. 53–86, 1991.

[52] C. R. Chu, M. B. Parlange, G. G. Katul, and J. D. Albertson, "Probability density functions of turbulent velocity and temperature in the atmospheric surface layer," *Water Resour. Res.*, vol. 32, pp. 1681–1688, 1996.